JOURNAL OF GEOPHYSICAL RESEARCH, VOL. 113, C04036, doi:10.1029/2007JC004360, 2008

Simulated heat storage in a perennially ice-covered high Arctic lake: Sensitivity to climate change

Aaron C. Vincent,[1,2] Derek R. Mueller,[3] and Warwick F. Vincent[1]

Received 26 May 2007; revised 12 October 2007; accepted 8 January 2008; published 26 April 2008.

[1] Perennially ice-covered, meromictic lakes occur along the northern coast of Ellesmere Island in the Canadian high Arctic and have distinctive conductivity and temperature profiles. They are salinity stratified and have deep thermal maxima that persist throughout the year at temperatures up to 60°C above the winter minimum in the overlying atmosphere. Heat transfer in one of these lakes (Lake A, latitude 83.0°N, longitude 75.4°W) was simulated using a high spatial resolution model based on a one-dimensional heat diffusion and radiative transfer equation, which was solved through numerical integration. Boundary conditions were forced using climate data from an automated weather station installed next to the lake. There was a good fit between simulated and observed water column temperatures, including the midwater temperature maximum of 8.5°C, after 63 years of heating (RMSE = 0.10°C). This suggests that Lake A became ice-free in the 1940s, a known period of intense warming of the circumpolar Arctic. The model was sensitive to forcing by photosynthetically active radiation (PAR, 400–700 nm), in addition to optically related parameters such as surface reflectance, snow and ice cover, and the PAR diffuse attenuation coefficient. The unusual thermal structure is affected by stratified layers of pigmented microbial communities, which enhance the absorption of solar radiation. Simulation of ice-free summers revealed that the lake's thermal profile would lose its characteristic shape over several decades and that ongoing climate change could reduce the thermal maximum from 8.5° to 4°C within 50 years.

Citation: Vincent, A. C., D. R. Mueller, and W. F. Vincent (2008), Simulated heat storage in a perennially ice-covered high Arctic lake: Sensitivity to climate change, *J. Geophys. Res.*, *113*, C04036, doi:10.1029/2007JC004360.

1. Introduction

[2] Lakes at temperate latitudes experience large seasonal fluctuations in the distribution and fluxes of heat within their water columns. In contrast, the perennially ice-covered lakes found at high latitudes can store heat in excess of the annual surface heat budget and can attain temperatures well above mean summer air temperatures, giving rise to deep subsurface thermal maxima. Shifts in ice cover associated with climate change are known to result in major impacts on high-latitude aquatic ecosystems [*Spigel and Priscu*, 1998] but little attention has been given to effects on the thermal regime of lakes with thick, multiyear ice cover.

[3] Perennially ice-covered lakes are common in coastal Antarctica and also found at the highest latitudes of the Arctic. The northern coastline of high Arctic Canada contains a series of meromictic (salinity stratified) lakes that retain their ice cover throughout most of the year. One of these lakes, named Lake A (Figure 1), was discovered in 1969 [*Hattersley-Smith et al.*, 1970; *Van Hove et al.*, 2006, and references therein], and like similarly stratified, ice-covered lakes nearby it has an unusual heat distribution. Specifically, Lake A has a deep thermal maximum in excess of 8°C despite mean surface air temperatures of only 3.3°C during July, the warmest month of the year (Alert, Nunavut climate normal 1971–2000, Meteorological Service of Canada). The potential responses of these ice-covered lakes to climate change are of particular interest given that, according to models and observation, the Arctic is experiencing the onset of severe climate change that is likely to accelerate over the course of this century [*Arctic Climate Impact Assessment* (*ACIA*), 2005; *Richter-Menge et al.*, 2006; *Serreze et al.*, 2000].

[4] The perennially ice-covered, meromictic lakes of Antarctica similarly display unusual thermal profiles; for example water column temperatures of up to 7.9°C in Lake Bonney and up to 25°C in Lake Vanda [*Spigel and Priscu*, 1998]. An analysis of these profiles has shown that they are likely the result of long-term solar heating [*Wilson and Wellman*, 1962]. This has been confirmed by static modeling efforts [*Hoare et al.*, 1964; *Shirtcliffe and Benseman*, 1964], however there has been no attempt to simulate their thermal properties by way of a dynamic model.

[5] The primary objectives of the present study were to evaluate the mechanisms responsible for the unusual tem-

[1] Centre d'Études Nordiques, Université Laval, Quebec City, Quebec, Canada.
[2] Now at Department of Physics, McGill University, Montreal, Quebec, Canada.
[3] Geophysical Research Institute, University of Alaska, Fairbanks, Fairbanks, Alaska, USA.

0148-0227/08/2007JC004360$09.00

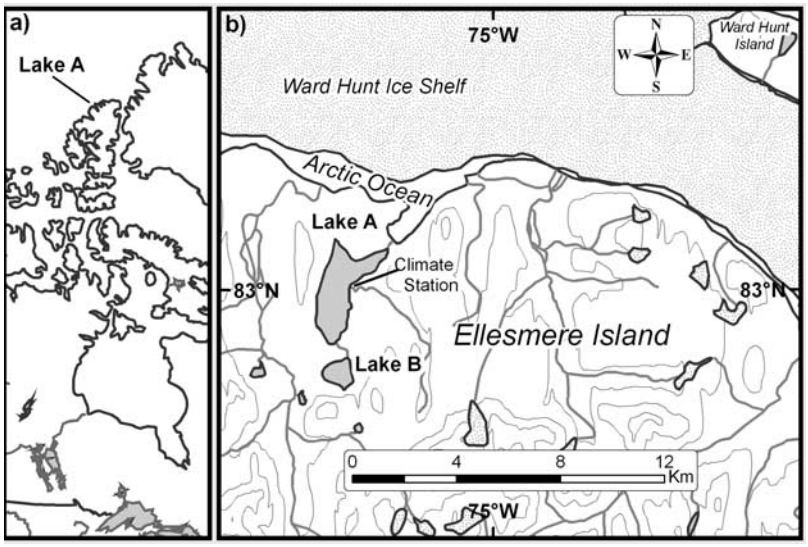

Figure 1. Map of the study site: (a) location of Ellesmere Island; (b) the Lake A drainage basin on Marvin Peninsula, northern Ellesmere Island. Note the position of the climate station.

perature profiles of perennially ice-covered polar lakes, and their sensitivity to environmental variables. To address these objectives, we developed a dynamic simulation model to analyze the heat fluxes in Lake A in the Canadian high Arctic. Model parameters were set based on our in situ observations of snow, ice and water properties, including depth profiles of salinity, temperature and optical variables. The model was forced using climate data from an automated weather station that we installed at the edge of Lake A. A secondary objective was to determine the duration of heating required to achieve the observed temperature maximum and profile shape of Lake A. Does the current temperature profile represents a steady state, or is it still evolving? We hypothesized that if the latter were true, the thermal structure may have been substantially disrupted during a warm period that was recorded in the circumpolar regions during the 1930s and 1940s. Our final objective was to evaluate the implications of climate change and the loss of ice cover on the thermal structure of the lake.

2. Methods

2.1. Environmental Observations

[6] Profiles of Lake A temperature and salinity were taken through holes in the ice and were referenced to the hydrostatic water level. Conductivity-temperature-depth profiling to 125 m (near the maximum depth of the lake) was performed in 2006 with an XR-420-CTDm (RBR Inc., Ottawa, ON, Canada) at a 1 Hz sampling rate, and to 48 m in 2001 using a Hydrolab Surveyor 3 (Hydrolab Corp., Austin, Tex.) at a sampling interval of 50 cm. In the 2001 profile, an under-ice localized thermal maximum of 4.7°C was removed prior to model forcing to avoid interpolation errors. This profile was extended from 48 m to a depth of 125 m using a logistic model fit to the 2006 data set. Temperatures were biased in the uppermost portion (top 1.4 m) of the 2006 profile before the instrument gained thermal equilibrium with the water column. To remove this artifact, these first 15 temperature data points were set to 1.17°C.

[7] Air temperature, humidity, net and photosynthetically active radiation (PAR; 400–700 nm) as well as wind speed and direction were recorded at an automatic climate station that we installed at 83.0023°N, 75.3896°W, 10 m from Lake A. Measurements were taken every minute by a Campbell Scientific CR10X data logger and output as hourly averages for a yearlong period beginning on 6 August 2004. During several periods totaling 76 days, when the wind speed was constantly zero (presumably due to anemometer ice riming), we substituted a predicted wind speed using a multiple regression analysis obtained by comparing available data at Lake A with wind data from Ward Hunt Island (15 km to the northeast).

2.2. Theory

[8] Two mechanisms were assumed to be responsible for heat transfer within the lake: absorption of solar radiation during the summer period, and heat conduction within the lake and ice cover. The radiation that can penetrate the snow and ice roughly corresponds to the PAR region of the spectrum, since the diffuse attenuation of light in pure ice increases by two orders of magnitude between 700 and 1400 nm [*Perovich*, 1996]. UV radiation (280–400 nm) accounts for less than 5% of the total incident radiation and is strongly reflected and attenuated by snow cover [*Vincent et al.*, 2007]. Therefore both UV and longwave radiation were assumed to be completely lost at the surface, with only PAR penetrating through the lake ice cover into the water column.

[9] Turbulent mixing was considered to be negligible through most of the water column for two reasons: (1) yearlong ice cover prevents wind-driven mixing and (2) a high salinity gradient [*Ludlam*, 1996] provides a density stratification that prevents gravity-driven convective mixing. Water is fresh just below the ice, and steadily increases in salinity to a maximum of 32 psu at the bottom of the lake.

[10] We applied the one-dimensional heat diffusion equation as in *Flato and Brown* [1996] and *Duguay et al.* [2003]

Table 1. Notation and Units for the Model Variables[a]

Symbol	Description	Units
C_T	stability-dependent bulk transfer coefficient	dimensionless
E_0	PAR irradiance	W m^{-2}
e_s	saturation vapor pressure	Pa
F_0	stored heat flux	W m^{-2}
F_i	PAR flux (at depth)	W m^{-2}
F_L	latent heat flux to water	W m^{-2}
K_d	PAR attenuation coefficient	m^{-1}
Q	heat absorbed	W m^{-2}
q	specific humidity	g kg^{-1}
Q_*	net radiation flux	W m^{-2}
Q_e	latent heat flux	W m^{-2}
Q_h	sensible heat flux	W m^{-2}
T	Temperature	K/°C
t	Time	s
U	wind speed	m s^{-1}
z	Depth	m

[a]PAR, photosynthetically active radiation.

with an additional forcing term that accounts for heat absorption from solar radiation:

$$\rho c \frac{\partial T(z,t)}{\partial t} = k \frac{\partial^2 T(z,t)}{\partial z^2} + K_d(1-r)E_0 e^{-K_d z}, \quad (1)$$

where ρ is the density, c is the specific heat, k is heat conductivity, $T(z, t)$ is the temperature, E_0 is the incoming penetrating PAR above the surface of the snow (we follow the symbolic convention for irradiance given by *Sakshaug et al.* [1997]), K_d (m^{-1}) is the diffuse attenuation coefficient of shortwave radiation (PAR), r is the proportion of PAR that is reflected by the snow and ice layer and t and z are time and depth, respectively. See Table 1 for a complete list of variables used in the model. Radiation attenuated by K_d was taken to be completely absorbed as heat. The value of K_d in snow was computed from the in situ snow-clearing experiments of *Belzile et al.* [2001]. Standard values for k were used for water and ice, however we estimated the thermal conductivity of snow from snow density using the empirical formula in *Sturm et al.* [1997].

[11] Three distinct layers (Figure 2) were considered: surface snow (0.5 m thick) [*Belzile et al.*, 2001], surface ice (2 m thick) [*Belzile et al.*, 2001], and finally lake water (122.5 m deep), which was salinity- and density-stratified. Diffuse attenuation (K_d) within the water column varies substantially with depth and was approximated (inset, Figure 7) by a parabolic (upper water column) and declining exponential (lower water column) fit to the attenuation data in *Belzile et al.* [2001].

[12] Surface heat flux F_0 can be estimated by subtracting the sensible and latent heat flux (Q_h and Q_e, respectively) from the net radiation (Q_*, which includes downwelling and upwelling radiation from 300 nm to 30 μm):

$$F_0 = Q_* - Q_h - Q_e. \quad (2)$$

The latter terms were parameterized as in *Ebert and Curry* [1993]:

$$Q_h = \rho_{\text{air}} c_{p,\text{air}} C_T U (T_0 - T_{\text{air}}), \quad (3)$$

$$Q_e = \rho_{\text{air}} L_v C_T U (q_{\text{sat}}(T_0) - q_{\text{air}}), \quad (4)$$

where L_v is latent heat of vaporization, U is wind speed, q is specific humidity, and c_p is the specific heat at constant pressure. The dimensionless bulk transfer coefficient was set to $C_T = C_{T0}$, the neutral stability coefficient, which assumes the Richardson number = 0 [*Oke*, 1987]:

$$C_{T0} = \frac{\kappa^2}{\ln(h/\sigma)}, \quad (5)$$

where h is instrument height in meters, taken here as 2.8 m, midway between the anemometer (3 m height) and other

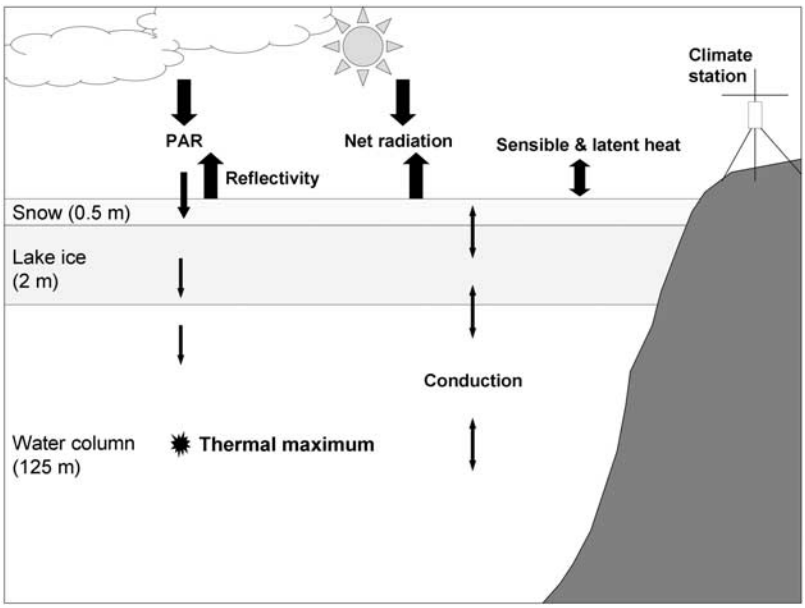

Figure 2. Diagram of the model fluxes.

Table 2. Symbols, Values, and Units of the Model Parameters and Constants

Symbol	Parameter	Values Used for Simulation	Units
		Model Parameters	
σ	surface roughness	0.00016	m
h	instrument height	2.8	m
i	depth increment (Δz)	0.331	m
j	time increment (Δt)	7.2	hours
r	reflectivity	0.7	dimensionless
v	ablation	1	m a^{-1}
z_{ice}	ice layer thickness	2	m
z_{snow}	snow layer thickness	0.5	m
z_{water}	water depth	122.5	m
θ	implicitness	1	dimensionless
		Constants	
c	specific heat	c_{air}, 1005; c_{water}, 4200; c_{ice}, 2090	J kg^{-1} K^{-1}
k	thermal conductivity	k_{snow}, 0.068 (at ρ = 210); k_{ice}, 2.13; k_{water}, 0.6	W m^{-1} K^{-1}
L_f	latent heat of fusion	0.335	MJ kg^{-1}
L_v	latent heat of vaporization	2.26	MJ kg^{-1}
ρ_{snow}	snow density	210	kg m^{-3}
ρ_{ice}	ice density	920	kg m^{-3}
g_i and g_5	saturation vapor coefficients	22 and 0.67	
g	acceleration due to gravity	9.8	m s^{-2}

sensors (2.6 m height), and σ is surface roughness (0.16 mm), also in meters; $\kappa = 0.4$ is von Karman's constant.

[13] Saturation vapor pressure was computed as

$$\ln e_s = \sum_{i=0}^{4} g_i T^{i-1} + g_5 \ln T, \tag{6}$$

where g_i and g_5 are the coefficients over ice given by *Hardy* [1998]. Latent heat was handled analogously to *McKay et al.* [1985], where ice thickness is static and an average rate of ice formation v is assumed. The rate of ablation is assumed, on an annual basis, to be equal to the rate of ice formation. Therefore, constant heat flux F_L due to latent heat at the ice-water interface takes the form

$$F_L = \rho v L_f, \tag{7}$$

where L_f is the latent heat of fusion of water. Temperature at the ice-water interface ($z = Z_{snow}$) was kept at constant 0°C.

[14] Despite the high level of density stratification in the lower water column, the fresh surface water is not density-stratified. A small amount of mixing was simulated by averaging water temperatures over approximately 60 cm below any local density maximum, if it occurred in the top 15 m of the water column.

2.3. Model and Forcing

[15] To solve the differential equation (1) we used a fully implicit in time, centered in space finite element algorithm similar to that of *Maykut and Untersteiner* [1971] for sea ice, adapted here to the entire snow-ice-water column. When this is converted to a difference equation it takes the form

$$\frac{T_i^{j+1} - T_i^j}{\Delta t} = (\Delta z)^{-2} \left\{ \left\langle \frac{k}{\rho c} \right\rangle_i \left(T_{i+1}^{j+1} - T_i^{j+1} \right) - \left\langle \frac{k}{\rho c} \right\rangle_{i-1} \left(T_i^{j+1} - T_{i-1}^{j+1} \right) \right\} - (\Delta z)^{-1} \frac{E_{i-1} - E_i}{\langle \rho c \rangle_i}. \tag{8}$$

Lower indices stand for depth in increments of Δz and upper indices stand for time in increments of Δt. Here the implicitness parameter [*Flato and Brown*, 1996] has been set to 1. The brackets $\langle\ \rangle_i$ denote a weighted average between z_{i-1} and z_i; that is,

$$\langle f(z) \rangle_i = \frac{\int_{z_{i-1}}^{z_i} f(z) dz}{z_i - z_{i-1}}. \tag{9}$$

All physical parameters that changed with depth were thus averaged within each element to minimize aliasing effects. The last term accounts for solar radiation where E_i is the flux of penetrating PAR at depth z_i. Density at each depth was calculated using an algorithm from *Fofonoff and Millard* [1983]. To solve equation (8), we used a matrix method similar to the one used by *Flato and Brown* [1996].

[16] The model was forced using the yearlong record of PAR and net radiation, wind speed, relative humidity and surface temperature data from the shore of Lake A. Hourly values for each climate variable were interpolated to each time increment using a cubic spline scheme.

[17] The model was numerically converged in order to make sure that numerical parameters did not influence the simulation results. Adequately small discrete element sizes were found to be approximately 7 hours for the time step and 31 cm for the water column depth elements, giving rise to 400 finite element points, which were evenly distributed though the model. The fully implicit scheme meant that there were no restrictions on these parameters, thus eliminating the divergences that occur when solving the diffusion equation with an explicit scheme [*Flato and Brown*, 1996].

[18] Using physical parameters identical to those measured at Lake A, the simulation was iterated over several hundred years. Beginning with a uniform temperature distribution (−1°C snow and ice, 4°C water column), the temperature throughout the 125-m water column was left to evolve over annual heating and cooling cycles.

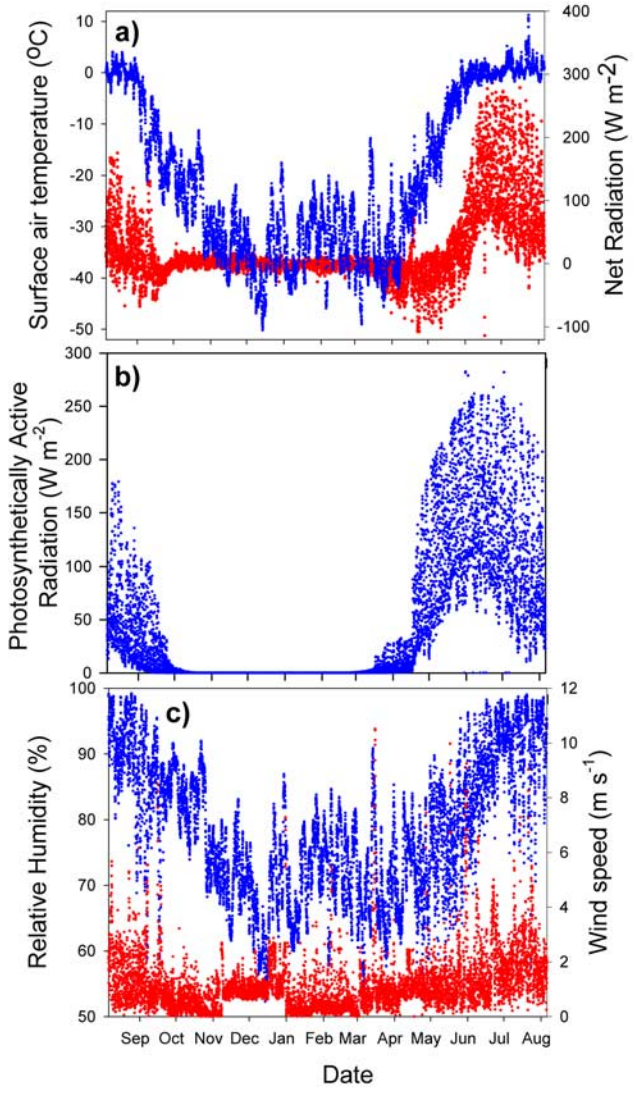

Figure 3. Climate forcing variables measured from August 2004 to August 2005: (a) surface air temperature (blue) and net radiation (red); (b) observed photosynthetically active radiation (PAR); (c) relative humidity (blue) and wind speed (red).

2.4. Model Validation

[19] The simulated temperature profile was compared to the reference temperature profile after it had been interpolated to the same depth increments as the model and shifted to account for the difference between hydrostatic water level and the top of the snow. We evaluated model performance by examining the RMSE of the simulated temperature profile at depths between 10 and 80 m. These thresholds were chosen since the temperature is close to invariant below 80 m and highly (seasonally) variable above 10 m. The best possible fit between the simulated and observed profiles was obtained when the simulated profile was shifted by a multiple of Δz (causes of this offset are discussed below). The best possible fit to the 2006 temperature profile (using the model simulation with observed parameters, the simulation time to best fit and the depth offset mentioned above) was used as a benchmark for further model analysis.

[20] A sensitivity analysis was performed by varying model parameters (Table 2) by at least 15% of their observed value and resimulating the water column profile. These model outcomes were evaluated based on the temperature (T_{max}) and depth (D_{max}) of the thermal maximum as well as the overall shape of the profile as compared to the 2006 observed profile (RMSE). Changes in the forcing variables were also assessed in a similar fashion to the parameters.

2.5. Loss of Ice Cover and Temperature Profile Recovery

[21] To simulate the impact of the loss of a summer ice cover, several simulations were run to mimic the effect of wind-induced turbulence in the water column. This was accomplished by reassigning the temperature in the 'mixed' upper water column to the mean temperature across these depths after each time step during July and August. In this manner, heat was conserved but the temperature distribution was altered. This simulation did not alter the salinity profile, the radiative transfer, surface energy balance or heat diffusion through the ice and snow layers.

[22] To simulate the recovery of the lake's profile from a mixing event, the model was initialized using the temperature profile observed in 2001 after the loss of ice cover in late August 2000. The model was allowed to evolve for several decades and simulated profiles were compared to the 2006 profile. Depth offsets between simulated and observed temperature profiles were not applied to model runs involving mixing and profile recovery.

3. Results

3.1. Physical Observations

[23] The average air temperature at Lake A for the period August 2004–2005 was −19.9°C with 69 thawing degree days and 7344 freezing degree days. The extreme values for hourly temperatures were 11.2°C in July and −50.2°C in December (Figure 3a). The annual average net radiation was 19.5 Wm^{-2} (range: −114–313 W m^{-2}; Figure 3a) and the average PAR received was 41 W m^{-2} (range: 0–282 W m^{-2}). Hourly average wind speeds ranged from 0 to 10 m s^{-1} and averaged 1.15 m s^{-1} over the measurement period (Figure 3c). Relative humidity ranged from 52 to 99% and averaged 78% (Figure 3c).

[24] The yearlong record of climate variables recorded at Lake A showed similarities to other nearby climate stations. The Environment Canada climate station at Alert, Nunavut has a continuous climate record from July 1951 and is 175 km to the east of Lake A. During the months in common with the Lake A record the annual temperature at Alert was −17.9°C, with 178 thawing degree days and 6702 freezing degree days (Meteorological Service of Canada). The most recent climate normal data for Alert (1971–2000) indicated an annual temperature of −18.0°C, therefore the measurement period was not anomalous in this respect relative to this 30-year reference period. The warmer conditions at Alert are consistent with our previous comparisons with the Ward Hunt Island region [*Mueller et al.*, 2003].

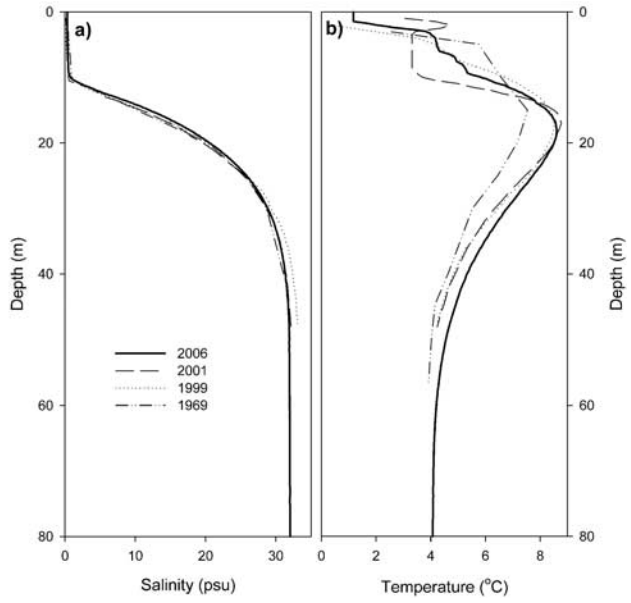

Figure 4. Lake A water column profiles: (a) salinity profiles; (b) temperature profiles. Note that the 2001 profile indicates prior mixing to a depth of 9 m. The 1969 profiles were obtained from *Hattersley-Smith et al.* [1970].

[25] The salinity profiles from Lake A over the period 1969 to 2006 demonstrate the stability of the water column, particularly in the section below 15 m in depth (Figure 4a). Temperature profiles from Lake A also showed the stability of the lower water column and the evolution of the thermal maximum over time (Figure 4b). Note that the 2006 thermal maximum is not the highest on record and that the constant temperatures in the upper ~9 m of the 2001 profile suggest a prior near-surface mixing event as discussed by *Van Hove* [2005].

[26] The 2006 temperature data were acquired in a descending fashion. The D_{max} of ascending Lake A profiles taken in 2003, 2004 and 2005 were on average 1.3 m higher than the descending profiles (W. F. Vincent, unpublished data, 2008). In addition the T_{max} of these profiles were 0.07°C cooler than their descending counterparts. This commonly observed hysteresis is due to the equilibration time of the thermistors and its implications are discussed below.

3.2. Dynamic Simulation of Heat Storage

[27] The simulations using the observed parameter values show the evolution of the temperature profile through time and the accumulation of heat in the mid water column (Figure 5a). The first important result is that the temperature of the current (2006) thermal maximum was reached following 63 years of simulation time. It should be noted that this temperature distribution does not correspond to a steady state according to our model. The maximum temperature continued to increase asymptotically toward a ceiling value of 10.62°C as heat accumulated in the water column, and the depth of the thermal maximum also increased (Figure 5a). The stepped form taken by the evolution of the depth of the thermal maximum is an artifact due to the spatial resolution (Δz) of the model. Simulation over longer time periods implied a slightly higher temperature maximum (11.5°C). The latter migrated slowly but linearly downward with time, reaching a depth of 20 m after 1000 years of simulation time, 25 m after 3000 years and 30 m after 5000 years.

3.3. Model Fit With Observed Parameters

[28] The best fit to the observed data was obtained after 63 years. At this time, the simulated temperatures at 10 m and below gave an extremely close fit to the measured profile (with the above mentioned offset of −1.88 m). This simulated profile had a T_{max} of 8.49°C and a D_{max} of 19.1 m (accounting for the offset), which matched closely to the

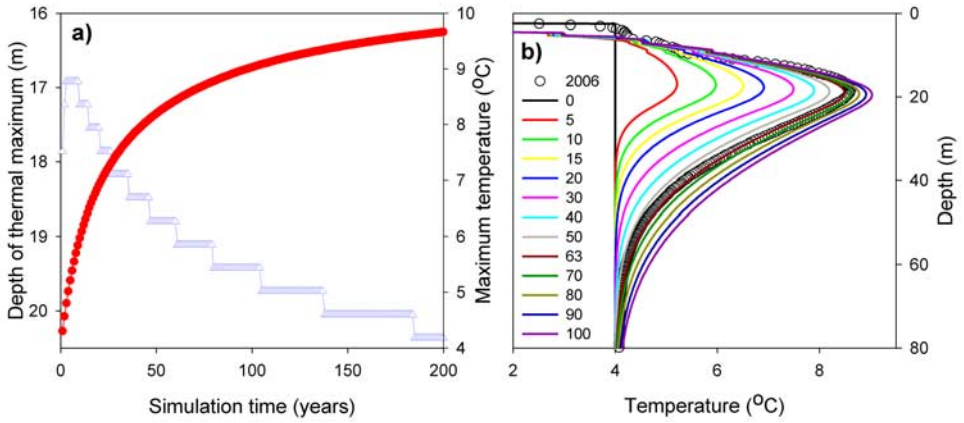

Figure 5. Simulated temperatures from the model using observed parameters: (a) simulated maximum temperature (filled circles) and D_{max}, the depth of maximum temperature; (b) simulated temperature profiles and fit to the 2006 water column profile using observed parameters for Lake A. Temperature profiles are starting at 4°C and evolving over the simulation time (year of each profile in legend). The simulated profiles were shifted downward by 1.88 m to best match the observed water column temperatures from 2006 (open circles) obtained with the conductivity-temperature-depth profiler.

2006 observed T_{max} of 8.60°C and D_{max} of 18.15 m. For the region of maximum heating, 10–80 m, the RMSE was only 0.10°C. Without offsetting the simulated temperature profile downward the best fit was obtained after 70 years of simulation time and had a T_{max} of 8.62°C, a D_{max} of 17.2 m and an RMSE of 0.24°C (more than double that of the offset simulation).

3.4. Model Sensitivity to Parameters

[29] Parameters which influenced the forcing term of equation (1) contributed the most to changes in the temperature distribution. Atmospheric conditions, as well as thickness, transparency and reflectivity of the snow and ice cover all had a large effect. Reducing the ratio of absorbed versus diffused heat made the temperature curve flatter and more homogeneous, whereas higher radiation gave a temperature maximum that lay closer to the surface, as radiative heating dominated over heat diffusion downward.

[30] Parameter sensitivity analysis (Figure 6) indicated that the model was most sensitive to the PAR attenuation coefficient (K_d) and reflectivity (r) where changes in the value of these parameters by small amounts (<5%) caused drastic changes in the shape of the simulated profile and T_{max}. The particular distribution of the diffuse attenuation coefficient K_d is crucial to the shape of the temperature distribution. A constant value throughout the water column gives a much flatter, slowly decreasing temperature profile, illustrated in Figure 7. The observed K_d, which varied with depth (water column mean = 0.198 m^{-1}, SD = 0.09 m^{-1}), gave the best fit (Figure 6a, large symbols), whereas the lowest RMSE was obtained with a K_d of 0.23 m^{-1} that did not vary with depth (Figures 6a and 7). The attenuation coefficient also governed D_{max} more than any other parameter due to the form of the Beer-Lambert equation. Reflectivity controlled the amount of PAR that penetrated the ice cover and, consequently, the addition of heat to the water column. The model time step affected the fit of the profile, T_{max} and D_{max} in a nonsystematic fashion (Figure 6c) and this is likely due to aliasing of the diel cycle by the cubic spline interpretation from hourly data. A similar nonlinear shift in D_{max} can be seen in response to changes in ice layer thickness (Figure 6d), especially when shifts are large but do not exceed a discrete depth element (Δz). This artifact is caused when the fraction of snow or ice at a single upper depth element goes to zero, and rounding errors make the weighted average of physical constants in this layer diverge, resulting in a shift in D_{max}, changes in T_{max} and a reduction in the model fit. We manually adjusted parameters to avoid this effect in the simulations, but a more systematic approach would be to vary the resolution of the model to keep the ice-water interface at a constant location within the numerical element. The thickness of the snow layer controls the amount of light entering the water column owing to its large K_d of 2.1 m^{-1} (Figure 6e). The ablation rate of the ice cover controls the amount of latent heat added into the water column directly below the ice and therefore a higher ablation rate raises T_{max} slightly and changes the shape of the profile by changing the heat diffusion in the water column (Figure 6g).

[31] Certain parameters did not affect the model performance substantially. These parameters were related to the sensible and latent heat in the surface energy budget and included the surface roughness (σ) and the instrument height (h). Variation in these parameters up to 15% did not influence the T_{max} or D_{max} and changed the RMSE by less than 1% of the benchmark value of 0.10. Of all the forcing variables, PAR was found to be the most important (Figure 8), followed by the reflectivity parameter (Figure 6b). Varying total incident PAR by as little as 5% made it impossible to achieve the correct shape. Substantial air temperature shifts affected the model outcome slightly with higher temperatures causing the T_{max} and RMSE to be reduced relative to the benchmark (Figure 6h). This may be due to a change in heat diffusion that altered the temperature profile. However, these changes were small (T_{max} shift of 0.06°C relative to the forcing change of 10°C), which underscores the importance of solar heating over direct heating for the lake. The remainder of the forcing variables (wind velocity, relative humidity, ablation rate) changed the RMSE by at most a few percent, the T_{max} by <0.03°C, while D_{max} remained unaltered.

3.5. Simulated Loss of Ice Cover and Temperature Profile Recovery

[32] The simulated effects of summertime ice loss and consequent wind-driven mixing were pronounced. Both the T_{max} and D_{max} decreased over simulation time as heat was dissipated both upward and downward from the thermal maximum. The initial rate of temperature change was highest for mixing depths greater than 5 m (Figure 9) but the rate of change leveled off for all mixing depths after ~50 years of simulation time. After 100 years, the model predicted a thermal maximum of 7.7°C for a mixing depth of 5 m, 4.9°C for a mixing depth of 10 m and 4.3°C for a mixing depth of 15 m. The temperature peak was greatly reduced in sharpness and it completely disappeared after 25 years of mixing down to 10 m, and after only 10 years of mixing down to 20 m (Figure 9).

[33] The model predicted the main features of the observed recovery from the upper water column mixing prior to 2001. Simulated temperatures decreased in the region of the thermal maximum, and D_{max} migrated to a position that was slightly lower in the water column. Meanwhile, heat from the thermal maximum diffused to higher and lower strata of the water column, leading to a broader peak. These features of the recovery can be clearly seen in the observed

Figure 6. Model sensitivity to parameters and forcing variables, showing changes in T_{max} (red squares), D_{max} (blue triangles), and the RMSE fit (black circles). (a) Constant values of diffuse attenuation coefficient K_d. Large symbols represent the realistic distribution of K_d in the water column, modeled after *Belzile et al.* [2001]. (b) Variations of incident PAR (which reflect changes in surface reflectivity) with respect to PAR measured at Lake A. (c) Variation of the numerical time step, showing PAR interpolation errors. (d) Variation of total ice thickness. (e) Variation of snow cover depth. (f) Variation of snow density. (g) Variation of ablation rate of ice at the ice-water interface, causing latent heat release. We used 1 m a^{-1}, as in *McKay et al.* [1985]. (h) Deviation in surface temperature with respect to measured climate data at Lake A.

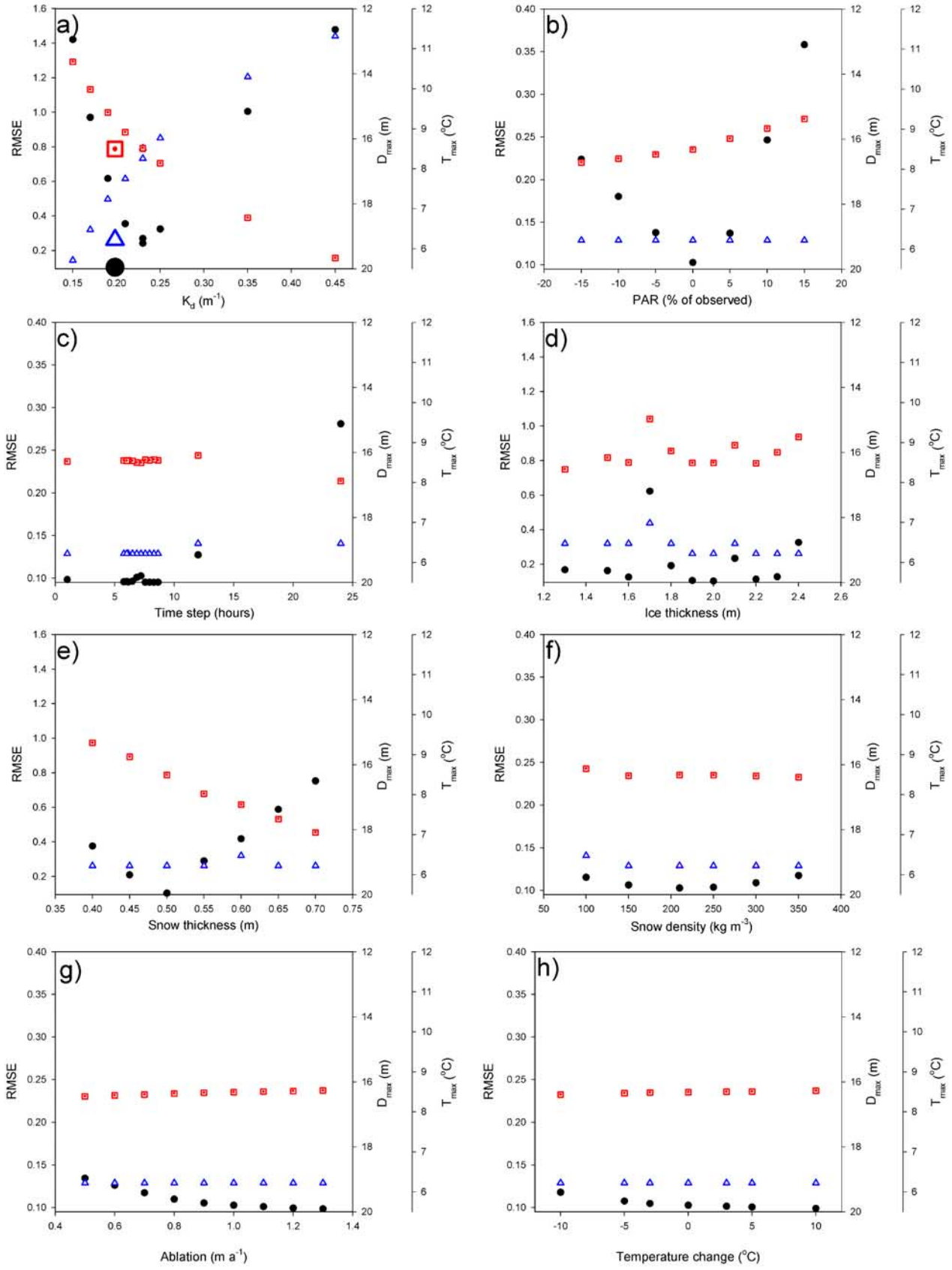
a)
b)
c)
d)
e)
f)
g)
h)
RMSE
D_{max} (m)
T_{max} (°C)
K_d (m^{-1})
PAR (% of observed)
Time step (hours)
Ice thickness (m)
Snow thickness (m)
Snow density (kg m^{-3})
Ablation (m a^{-1})
Temperature change (°C)

Figure 6

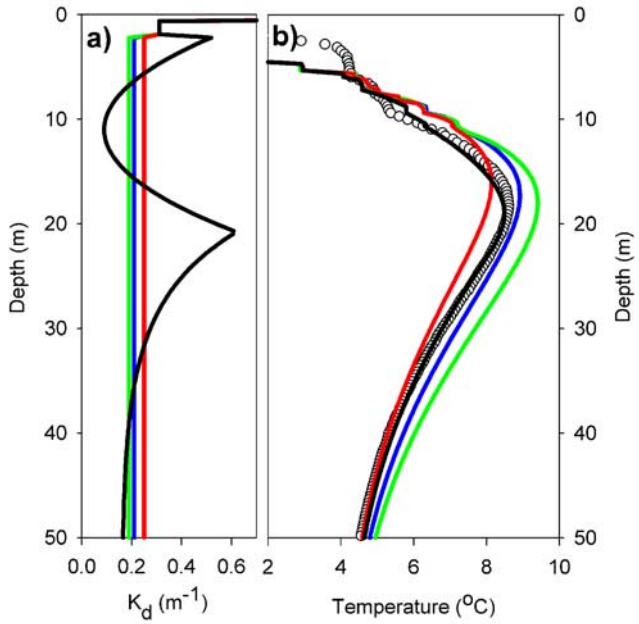

Figure 7. The effects of diffuse attenuation K_d changes on simulated water column profiles: (a) the K_d values approximated from *Belzile et al.* [2001] (black) and constant K_d values used to force the model; (b) observed temperature profile from 2006 (open circles) and the simulated profiles forced by respective K_d shown in Figure 7a (same symbols).

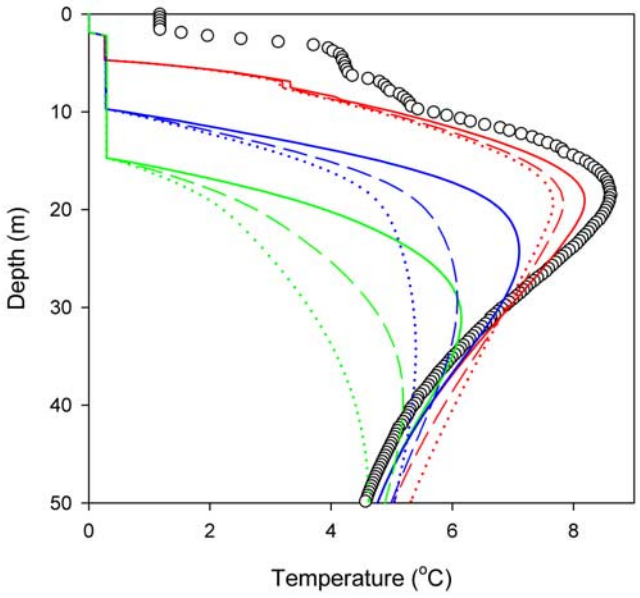

Figure 9. Model simulation of wind-driven mixing during July and August. The 2006 temperature profile data (open circles) and simulations of mixing to a depth of 5 m (red lines) after 10 (solid), 25 (dashed), and 50 (dotted) simulation years; mixing to a depth of 15 m (blue lines) after 10 (solid), 25 (dashed), and 50 (dotted) simulation years; and mixing to a depth of 20 m (green lines) after 10 (solid), 25 (dashed), and 50 (dotted) simulation years.

temperature profiles (Figure 10). However, the model underpredicted the temperature shift below the thermal maximum and overpredicted the temperature shift both above and within the thermal maximum region. As a result, the best fit to the 2006 profile for the recovery simulation

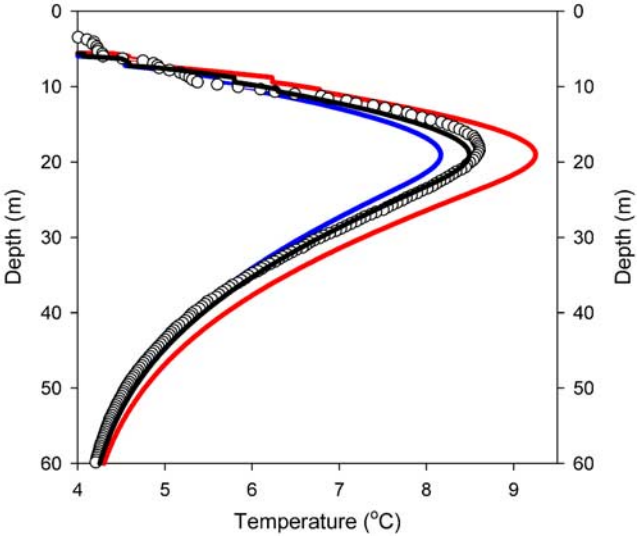

Figure 8. The effect of changes in PAR on simulated water column profiles: the observed temperature profile from 2006 (open circles), the simulated profile forced by observed PAR (black line), and profiles forced by 15% more PAR (red line) and 15% less PAR (blue line).

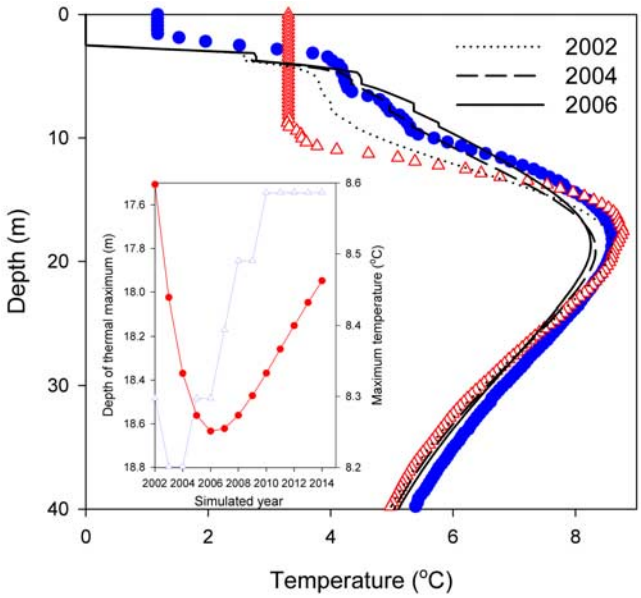

Figure 10. Simulated recovery of the Lake A temperature profile after a mixing event: the observed water column temperatures in 2001 mixed to a depth of ~9 m (open triangles), the observed profile in 2006 (solid circles), and the simulated recovery after 1 year (dotted line), 3 years (dashed line), and 5 years (solid line). Inset shows time evolution of thermal maximum temperature and depth in the lake.

was after 13 years (not shown) after the T_{max} started to increase again, with a depth offset of $-4\Delta z$ (-1.25 m).

4. Discussion

4.1. Model Validity

[34] The excellent fit of the simulated profile to the 2006 field data implies that the dominant mechanism responsible for the thermal profile of Lake A is absorption of solar radiation, corresponding to the forcing term in the heat diffusion equation (1). This is substantially different from lakes without year-round ice cover, since there is no wind-induced mixing to force heat loss through convection. This also suggests that it was reasonable to consider only absorption in the PAR range. Although latent heat fluxes and thermal diffusion through the ice-water interface do play a role, the simulations show that the most important parameters are those that affect PAR available for heating and absorbed as heat, which include the attenuation and reflection due to ice and snow cover, the attenuation coefficients due to absorption within the water, and the incident flux of radiation during the summer season.

[35] A critical variable affecting D_{max}, T_{max}, and the shape of the temperature profile was the attenuation coefficient K_d. This coefficient varies markedly as a function of depth in Lake A as a result of PAR-absorbing biological communities: phytoplankton populations in the surface waters under the ice and photosynthetic sulfur bacteria in the anoxic waters below 12 m [*Belzile et al.*, 2001]. This biological effect on the physical environment has been previously noted in the ocean where deep chlorophyll *a* maxima absorb heat and modify the thermal profiles [*Lewis et al.*, 1983].

[36] Although the model fit well to the observed temperature profile in 2006 the best fit was contingent upon shifting the depth of the simulated temperatures downward by 1.88 m. The need for this offset could be due to errors in the observed profiles as well as potential deficiencies in the model. A large part of this offset is likely due to the downward direction of the sampling and the thermal hysteresis of the thermistors mentioned above. Additionally, the model simulations of wind-driven mixing and recovery indicate that these perturbations lower D_{max} below its naturally evolving position (Figures 9 and 10); given the documented loss of ice cover in 2000 [*Van Hove*, 2005], it is possible that this mixing event (or earlier, unknown events) could have lowered D_{max}, thereby requiring an offset for model fitting. There are also likely to be seasonal and interannual variations in the optical properties of the lake and in the thickness and optical properties of its overlying ice and snow ice cover, which would affect D_{max}. Finally, *Shirtcliffe and Benseman* [1964] found a similar offset in Lake Bonney Antarctica, and hypothesized that it could be the result of a rise in water levels due to excess meltwater influx to the surface. However, this is a less probable explanation for Lake A, which unlike Lake Bonney has an outflow that removes excess water.

[37] The model developed here is likely appropriate to other ice-capped, solar heated lakes in the polar regions such as lakes B, C1, and C2 on Ellesmere Island in the Arctic and Lake Bonney and Lake Vanda in the McMurdo Dry Valleys, Antarctica. The latter Antarctic lakes have much thicker ice covers, which may be the result of their minimal cover of insulating snow relative to the Arctic lakes.

4.2. Simulated Thermal History

[38] The model simulated the development of the deep thermal maximum and implied that the currently observed profile could have been achieved within 60–70 years if model parameters and forcing variables remain relatively constant during this time. This suggests that the present thermal structure in Lake A only began to form in the 1940s. This simulation result is of great interest because a period of intense warming was observed throughout the Arctic in the 1930s and 1940s, accompanied by a pronounced decrease in sea ice extent off Eurasia [*ACIA*, 2005]. Large changes also likely occurred along the northern coastline of Ellesmere Island at this time, including substantial breakup and loss of the Ellesmere Ice Shelf [*Vincent et al.*, 2001]. During this period, Lake A may have remained ice-free for an extended number of summer seasons. Assuming the salinity gradient was relatively unperturbed by this mixing event, the lake's upper 30 m may have cooled, providing "initial conditions" similar to the ones used in the simulation. Lower summer temperatures in subsequent decades with only a few ice-free years would then permit the formation of this unique thermal structure. The goodness of fit of the model suggests that these dynamic systems are quite insensitive to small perturbations. Any one-time event such as a single, unusually cold or warm year would have been smoothed out over the lake's history.

4.3. Future Evolution of the Lake

[39] The model results show that ice melting associated with an increase in atmospheric temperatures would result in a gradual loss of the unique thermal structure of Lake A and a decrease in its water column temperatures. It would, however, take a large number of ice-free summers to lose the curve's characteristic shape entirely, suggesting that the system is not overly sensitive to small perturbations. This is further evidenced by the simulated and observed recovery of the heat profile after the 2000 mixing event. Our simulation of wind-induced mixing during ice-free summers was a coarse approximation, based on a simple averaging of temperatures. However, the magnitude of effect will depend on the depth, frequency and intensity of mixing. Accompanying changes in ice cover thickness, the salinity profile, and dynamic convective processes will further modify these effects, but would be difficult to capture in a one-dimensional model. These elements are most likely responsible for the disparity between the simulated and observed recovery that took place between 2001 and 2006. Over long time periods, the boundary conditions in the bottom of the lake (assumed to be a bottomless heat sink in our model) may become important as the temperature gradient at the bottom of the lake grows. It is clear, however, that extended periods of ice-free summers would result in significant loss of thermal energy from the lake, and could eliminate completely the deep-water temperature peak. This would have profound implications for the microbial communities that have developed within this deep-water maximum.

5. Conclusions

[40] Perennially ice covered lakes are known to be the habitats for diverse, highly structured biological communities that are organized along the vertical gradients in

temperature, salinity and associated chemical variables. Our results show that the remarkable thermal gradients of one such lake, Lake A, at the extreme north of the Canadian high Arctic, can be accurately modeled by a one dimensional heat diffusion and radiative transfer equation. Continuous net solar heating takes place because ice prevents the escape of heat through wind-induced convective cooling. This greenhouse effect gives rise to temperatures within the water column in great excess of the mean summer temperatures above the ice. The close goodness-of-fit to observed data show that equation (1) and the appropriate boundary conditions constitute an accurate model of this physical system.

[41] The model is highly sensitive to changes in the variables that affect PAR (the forcing term): incoming radiation, attenuation by snow and ice, and K_d, the diffuse attenuation coefficient in the water. This is an important biophysical feedback effect, where growth of pigmented microbes affects the local absorption of PAR, thereby causing an increased accumulation of heat in their surrounding waters. Boundary conditions such as heat loss through diffusion to the atmosphere, latent heat and wind-driven cooling of the snow have minimal but nonnegligible effects on the overall dynamics.

[42] Assuming no change in forcing, simulated time evolution of such a system indicates that it would take about 63 years to attain a temperature profile identical to the one observed in 2006. Results also show that the observed temperature profile in Lake A is not a steady state. Rather, it is still evolving after having recovered its yearlong ice cover following a series of warm years that were recorded in the Arctic in the 1930s and 1940s.

[43] The prolonged loss of ice cover due to climate change would have a drastic effect on Lake A. More than a decade of ice-free summers would cause the unique temperature profile to be completely lost due to wind-driven mixing. Ironically, the increased greenhouse warming on a planetary scale may bring about the collapse of the greenhouse effect in Lake A and other ice-covered polar lakes, thereby altering these ecosystems through cooling and completely disrupting their unique biophysical structure.

[44] **Acknowledgments.** We acknowledge the financial assistance from ArcticNet (a Canadian Network of Centres of Excellence), the Canada Research Chair in Aquatic Ecosystems Studies, and the Natural Sciences and Engineering Research Council of Canada (Discovery Grant to W.F.V. and postdoctoral fellowship to D.R.M.). The Arctic Regions Supercomputing Center supplied computational resources, and the Polar Continental Shelf Project provided logistical support for fieldwork (this is PCSP/ÉPCP publication 038-07). Our ongoing field studies in the Ward Hunt Island Observatory region are supported by Quttinirpaaq National Park and the Canadian Foundation for Innovation. Field assistance with water column profiling and climate observations was provided by Dermot Antoniades, Claude Belzile, Jeffrey Kheraj, Jérémie Pouliot, Antonio Quesada, Sébastien Roy, Denis Sarrazin, Jessica Tomkins, Patrick Van Hove, and Julie Veillette. We also thank an anonymous referee, Marlon Lewis, and Chris McKay for their insightful review comments and suggestions.

References

Arctic Climate Impact Assessment (ACIA) (2005), *Arctic Climate Impact Assessment*, 1042 pp., Cambridge Univ. Press, New York.

Belzile, C., W. F. Vincent, J. A. E. Gibson, and P. Van Hove (2001), Bio-optical characteristics of the snow, ice, and water column of a perennially ice-covered lake in the high Arctic, *Can. J. Fish. Aquat. Sci.*, *58*, 2405–2418.

Duguay, C. R., G. M. Flato, M. O. Jeffries, P. Ménard, K. Morris, and W. Rouse (2003), Ice-cover variability on shallow lakes at high latitudes: Model simulations and observations, *Hydrol. Proc.*, *17*, 3465–3483.

Ebert, E. E., and J. A. Curry (1993), An intermediate one-dimensional thermodynamic sea ice model for investigating ice-atmosphere interactions, *J. Geophys. Res.*, *98*, 10,085–10,109.

Flato, G. M., and R. D. Brown (1996), Variability and climate sensitivity of landfast Arctic sea ice, *J. Geophys. Res.*, *101*, 25,767–25,777.

Fofonoff, N. P., and R. C. Millard (1983), Algorithms for computation of fundamental properties of seawater, *Tech. Pap. Mar. Sci.*, *44*, 53 pp., UNESCO Div. of Mar. Sci., Paris.

Hardy, B. (1998), ITS-90 formulations for vapor pressure, frostpoint temperature, dewpoint temperature and enhancement factors in the range −100 to +100 C, paper presented at 3rd International Symposium on Humidity and Moisture, Natl. Phys. Lab., London.

Hattersley-Smith, G., J. E. Keys, H. Serson, and J. E. Mielke (1970), Density stratified lakes in northern Ellesmere Island, *Nature*, *225*, 55–56.

Hoare, R. A., K. B. Popplewell, D. A. House, R. A. Henderson, W. T. Prebble, and A. T. Wilson (1964), Lake Bonney, Taylor Valley, Antarctica: A natural solar energy trap, *Nature*, *202*, 886–888.

Lewis, M. R., J. J. Cullen, and T. Platt (1983), Phytoplankton and thermal structure in the upper ocean: Consequences of nonuniformity in chlorophyll profile, *J. Geophys. Res.*, *88*, 2565–2570.

Ludlam, S. D. (1996), The comparative limnology of high Arctic, coastal, meromictic lakes, *J. Paleolimnol.*, *16*, 111–131.

Maykut, G. A., and N. Untersteiner (1971), Some results from a time-dependent thermodynamic model of sea-ice, *J. Geophys. Res.*, *76*, 1550–1575.

McKay, C. P., G. D. Clow, R. A. Wharton, and S. W. Squyres (1985), Thickness of ice on perennially frozen lakes, *Nature*, *313*, 561–562.

Mueller, D. R., W. F. Vincent, and M. O. Jeffries (2003), Break-up of the largest Arctic ice shelf and associated loss of an epishelf lake, *Geophys. Res. Lett.*, *30*(20), 2031, doi:10.1029/2003GL017931.

Oke, T. R. (1987), *Boundary Layer Climates*, 2nd ed., 435 pp., Routledge, New York.

Perovich, D. K. (1996), The optical properties of sea ice, report, 25 pp., Dept. of the Army Corps of Eng. Cold Reg. Res. and Eng. Lab., Hanover, N. H.

Richter-Menge, J., et al. (2006), State of the Arctic, report, 36 pp., NOAA Pac. Mar. Environ. Lab., Seattle, Wash.

Sakshaug, E., A. Bricaud, Y. Dandonneau, P. G. Falkowski, D. A. Kiefer, L. Legendre, A. Morel, J. Parslow, and M. Takahashi (1997), Parameters of photosynthesis: Definitions, theory and interpretation of results, *J. Plankton Res.*, *19*, 1637–1670.

Serreze, M. C., J. E. Walsh, F. S. Chapin, T. Osterkamp, M. Dyurgerov, V. Romanovsky, W. C. Oechel, J. Morison, T. Zhang, and R. G. Barry (2000), Observational evidence of recent change in the northern high-latitude environment, *Clim. Change*, *46*, 159–207.

Shirtcliffe, T. G. L., and R. F. Benseman (1964), A sun-heated Antarctic lake, *J. Geophys. Res.*, *69*, 3355–3359.

Spigel, R. H., and J. C. Priscu (1998), Physical limnology of McMurdo Dry Valley lakes, in *Ecosystem Dynamics in a Polar Desert: The McMurdo Dry Valleys, Antarctica*, *Antarct. Res. Ser.*, vol. 72, edited by J. C. Priscu, pp. 153–187, AGU, Washington, D. C.

Sturm, M., J. Holmgren, M. König, and K. Morris (1997), The thermal conductivity of seasonal snow, *J. Glaciol.*, *43*, 26–41.

Van Hove, P. (2005), Limnologie du Nord d'île d'Ellesmere: Réponses et Sensibilité aux Changements de Climat dans les Environnements Extrêmes, Ph.D. thesis, 119 pp., Univ. Laval, QC, Canada.

Van Hove, P., C. Belzile, J. A. E. Gibson, and W. F. Vincent (2006), Coupled landscape-lake evolution in the coastal high Arctic, *Can. J. Earth Sci.*, *43*, 533–546.

Vincent, W. F., J. A. E. Gibson, and M. O. Jeffries (2001), Ice shelf collapse, climate change, and habitat loss in the Canadian high Arctic, *Polar Rec.*, *37*, 133–142.

Vincent, W. F., M. Rautio, and R. Pienitz (2007), Climate control of underwater UV exposure in polar and alpine aquatic ecosystems, in *Arctic Alpine Ecosystems and People in a Changing Environment*, edited by J. B. Orbaek et al., pp. 227–249, Springer, Berlin.

Wilson, A. T., and H. W. Wellman (1962), Lake Vanda: An Antarctic lake, *Nature*, *196*, 1171–1173.

D. R. Mueller, Geophysical Research Institute, University of Alaska, Fairbanks, 903 Koyukuk Drive, P.O. Box 757320, Fairbanks, AK 99775-7320, USA.

A. C. Vincent, Department of Physics, Rutherford Physics Building, McGill University, 3600 Rue University, Montreal, QC H3A 2T8, Canada. (vincenta@physics. mcgill.ca)

W. F. Vincent, Département de Biologie, Université Laval, Quebec City, QC G1V 0A6, Canada.